



Information for the Defense Community

DTIC® has determined on 12 / 4 / 2015 that this Technical Document has the Distribution Statement checked below. The current distribution for this document can be found in the DTIC® Technical Report Database.

DISTRIBUTION STATEMENT A. Approved for public release; distribution is unlimited.

© **COPYRIGHTED.** U.S. Government or Federal Rights License. All other rights and uses except those permitted by copyright law are reserved by the copyright owner.

DISTRIBUTION STATEMENT B. Distribution authorized to U.S. Government agencies only (fill in reason) (date of determination). Other requests for this document shall be referred to (insert controlling DoD office).

DISTRIBUTION STATEMENT C. Distribution authorized to U.S. Government Agencies and their contractors (fill in reason) (date determination). Other requests for this document shall be referred to (insert controlling DoD office).

DISTRIBUTION STATEMENT D. Distribution authorized to the Department of Defense and U.S. DoD contractors only (fill in reason) (date of determination). Other requests shall be referred to (insert controlling DoD office).

DISTRIBUTION STATEMENT E. Distribution authorized to DoD Components only (fill in reason) (date of determination). Other requests shall be referred to (insert controlling DoD office).

DISTRIBUTION STATEMENT F. Further dissemination only as directed by (insert controlling DoD office) (date of determination) or higher DoD authority.

Distribution Statement F is also used when a document does not contain a distribution statement and no distribution statement can be determined.

DISTRIBUTION STATEMENT X. Distribution authorized to U.S. Government Agencies and private individuals or enterprises eligible to obtain export-controlled technical data in accordance with DoDD 5230.25; (date of determination). DoD Controlling Office is (insert controlling DoD office).



Cornell University
College of Engineering

School of Civil and
Environmental Engineering
Peter Diamessis
Associate Professor
Environmental Fluid Mechanics and
Hydrology
105 Hollister Hall
Ithaca, NY 14853
Tel: 1-607-255-1719
Fax: 1-607-255-9004
e-mail: pjd38@cornell.edu
website: www.cee.cornell.edu/pjd38

Ithaca, NY, June 19, 2014

Defense Technical Information Center
8725 John J. Kingman Road Ste 0944
Fort Belvoir, VA 22060-6218

To Whom It May Concern:

Please find attached my final report for the O.N.R.-Turbulence and Stratified Wakes-funded project titled "Subsurface Signature of the Internal Wave Field Radiated by Submerged High Reynolds Number Stratified Wakes" (Award Number: N00014-08-1-0235). The enclosed document is a revised version of the original report sent on May 28th. The updated report contains figures that are all of journal quality. I apologize for the quality of the figures in the original document.

Please let me know if you would like any additional information from me.

Sincerely,

A handwritten signature in black ink, appearing to read "P. Diamessis".

Peter Diamessis

FINAL REPORT, May 26, 2014

Contract Information

Contract Number	N00014-08-1-0235
Title of Research	a) Internal Waves Generated by High Reynolds Number Stratified Wakes (2/1/2008 to 9/30/2010). b) Subsurface Signature of the Internal Wave Field Radiated by Submerged High Reynolds Number Stratified Wakes (10/1/2010 to 9/30/2013)
Principal Investigator	P. J. Diamessis
Organization	School of Civil and Environmental Engineering, Cornell University
Contracting Officer	Dr. Ronald Joslin

Technical Section

Technical Objectives

The research supported by ONR grant number N00014-08-1-0235 was conducted in two phases, as indicated above. The primary objectives of each phase are listed below.

STAGE-1, "Internal Waves Generated by High Reynolds Number Stratified Wakes":

- Characterize the internal wave field emitted by a stratified turbulent wake during the Non-Equilibrium (NEQ) regime and the particular modifications associated with high Reynolds numbers and the secondary instabilities therein.
- Determine the remote signature of the wake-radiated waves, as modeled by a 2-D internal wave beam, by examining their interactions with variations in the background stratification profile.

STAGE-2, "Subsurface Signature of the Internal Wave Field Radiated by Submerged High Reynolds Number Stratified Wakes":

- Characterize the low-wind-condition subsurface signature of a single high-frequency internal wave beam(s) in a uniform or vertically variable stratification, the latter typical of littoral ocean conditions.
- Correlate qualitatively and quantitatively, over a range of Reynolds and Froude numbers, the patterns of subsurface motion observed above a stratified turbulent wake with the flow patterns inside the wake core to infer the state ("age") of wake turbulence.

Results

The results obtained in pursuit of the above objectives may be grouped in the following categories, on each of which we further elaborate below:

1 20150925064

- (i) Mean flow generation and mitigation in large-amplitude internal wave packets.
- (ii) Interaction of an internal wave beam with a model oceanic pycnocline.
- (iii) Wake-emitted internal waves.
- (iv) Proper orthogonal decomposition of the wake-radiated internal wave field.
- (v) Eulerian mean flows during the reflection of an internal wave beam off a free-slip surface.
- (vi) Lagrangian mean flows and dispersion in a reflecting internal wave beam.
- (vii) Subsurface signature of the wake-radiated internal wave field.

(i) Mean Flows in Large-Amplitude Internal Wave Packets.

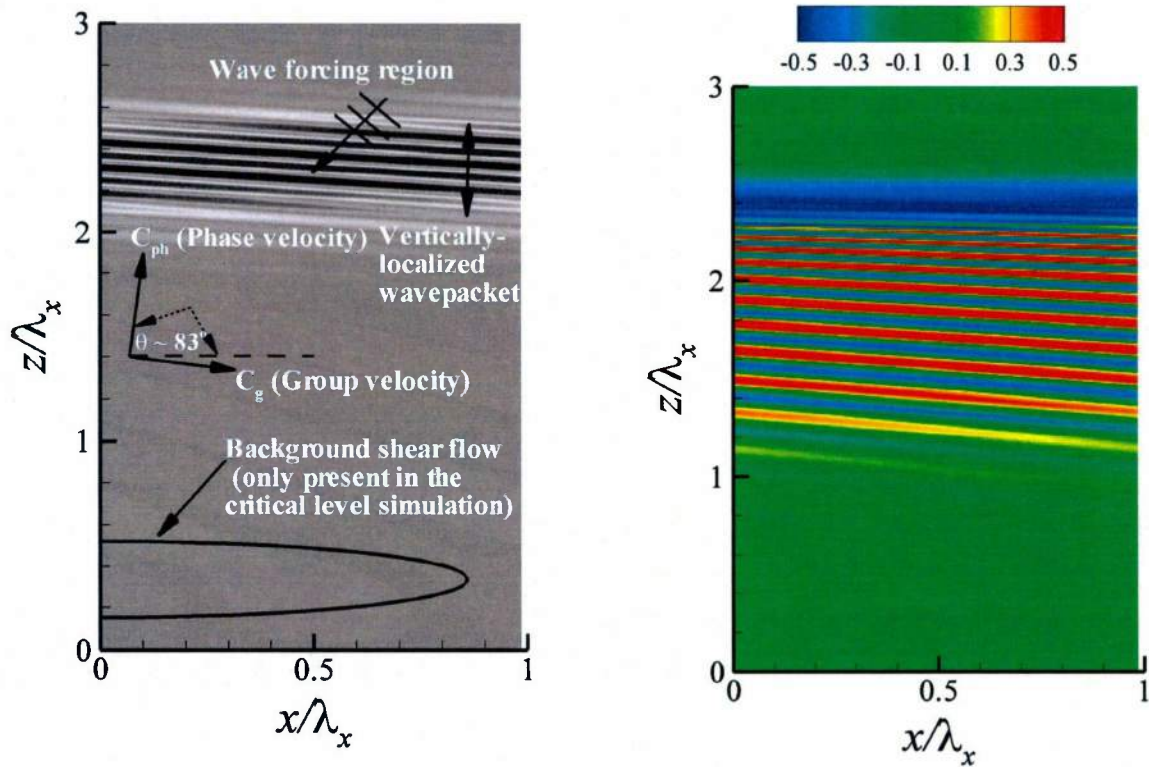


Figure 1: Left panel: Schematic of problem setup where a vertically localized IGW is generated in the forcing region and allowed to freely propagate downward. In the critical level simulation (described in greater detail in the Ph.D. thesis of A.M. Abdilghanie), a Gaussian background shear flow is positioned near the bottom of the computational domain. Right panel : Two-dimensional contours of the horizontal velocity field after five wave periods in a fully nonlinear simulation of a horizontally periodic vertically localized wave packet. The virtual wave-generator is located at $z/\lambda_x \approx 2.5$ where a significant mean flow is observed.

2-D internal wave beams (IWB) or packets are often used as idealized models for internal waves radiated by submerged topography in the ocean and the internal wave field emitted by a localized stratified turbulent event such a turbulent wake. Both IWBs and internal wave packets, nevertheless, carry some of the salient features of the above geophysical and naval internal wave fields, including their ability to support significant nonlinearity and dispersion.\

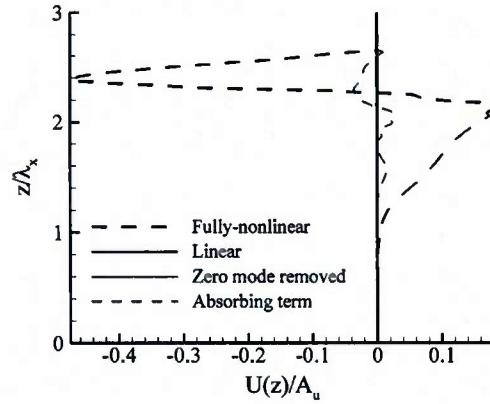


Figure 2: Comparison of the mean horizontal flow in a fully nonlinear simulation and linear simulations, along with simulations in which either the zero Fourier mode is removed or the proposed mean flow absorbing term is used, for a horizontally-periodic vertically-localized wave packet.

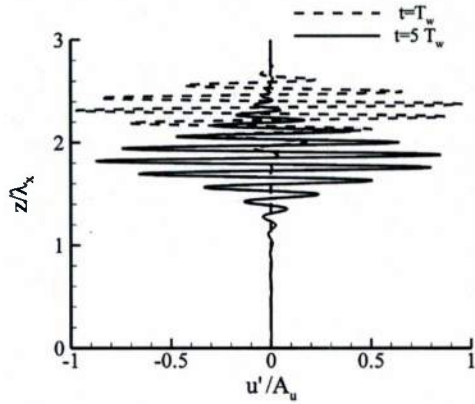


Figure 3: Vertical profile of the instantaneous horizontal velocity, sampled through the middle of a wave packet, compared at one and five wave periods in a fully nonlinear simulation of a horizontally periodic vertically localized wave packet in which the mean flow absorbing term is used.

Our very first effort within this ONR-funded project aimed to study the interaction of a finite-amplitude 2-D, horizontally non-localized internal wave packet, with a background shear layer, as shown in the left panel of Figure 1. Nevertheless, we found that our wave packet underwent significant distortion and decay as soon as it was generated ; it fully degenerated far from the source (right panel of the same figure). We established an understanding of the mechanism underlying this mean flow formation which was found to lie in the gradient of the vertical Reynolds stress field of the wave packet. A scaling of the strength of the mean flow as a function of wave amplitude, stratification characteristics and wave packet

localization was provided. This scaling was then used to construct various mean flow mitigation techniques to enable a robust wave-amplitude internal wave packet propagate sufficiently far from its source free of any mean flow (figures 2 and 3). This wave packet ultimately interacts with variations in background stratification in current. Such interactions are characterized by significant nonlinearity and can provide important insight into the remote fate of wake-radiated internal waves. More detail on this study may be found in the article by Abdilghanie and Diamessis (*Theor. and Comp. Fluid Dyn.* 2012).

(ii) Internal wave beam-pycnocline interaction

The driving question behind this particular investigation was whether a significant fraction of wake-radiated internal wave energy can propagate through variations in the ambient stratification profile. This work was conducted in close collaboration with Dr. Scott Wunsch at the Johns Hopkins U. Applied Physics Laboratory. Since the simulation of the interaction with an overlying pycnocline of the internal wave field radiated by an actual/full stratified full wake would be a prohibitively costly computational endeavor, we opted to focus on the interaction of an upward propagating internal wave beam (IWB) with a pycnocline above which also sits a mixed layer (see Figure 4 for a schematic of the computational domain and an example stratification profile).

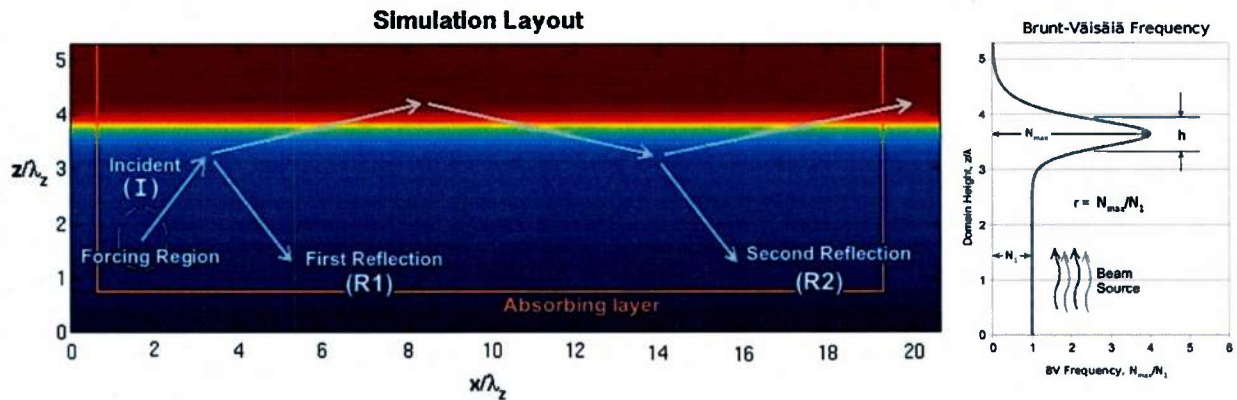


Figure 4: Left panel: Schematic of the computational domain indicating the dominant phenomena along the IWB trajectory: primary and secondary reflection and refraction. The color shading denotes the background density profile extending from light to heavy with increasing depth. Right panel: Example Brunt-Väisälä frequency profile showing the two fundamental parameters of the problem under consideration: Pycnocline thickness, h , and the ratio $r = N_{max}/N_1$ of maximum buoyancy frequency inside the pycnocline to its value in the lower layer.

Dr. Wunsch's equivalent experimental studies had revealed the formation of high amplitude harmonics upon encounter of the IWB with the pycnocline ; these harmonic waves were typically trapped inside the pycnocline and tended to propagate downstream within it. To this end, our numerical work also focused on harmonic formation. 24 simulations were conducted examining a range of pycnocline to lower layer buoyancy frequency ratios, $r = N_{max}/N_1$, and normalized pycnocline thicknesses h/λ_x , where λ_x is the IWB's horizontal wavelength. Our work was restricted to IWB propagation angles of 45° with respect to the horizontal, typical of what is observed in wake-radiated internal wave fields (see also section (iii)), and a beam with relatively high steepness of 2% . Such an IWB has sufficiently high amplitude to undergo a variety of nonlinear effects within the pycnocline but is not strong enough to be subject to breaking.

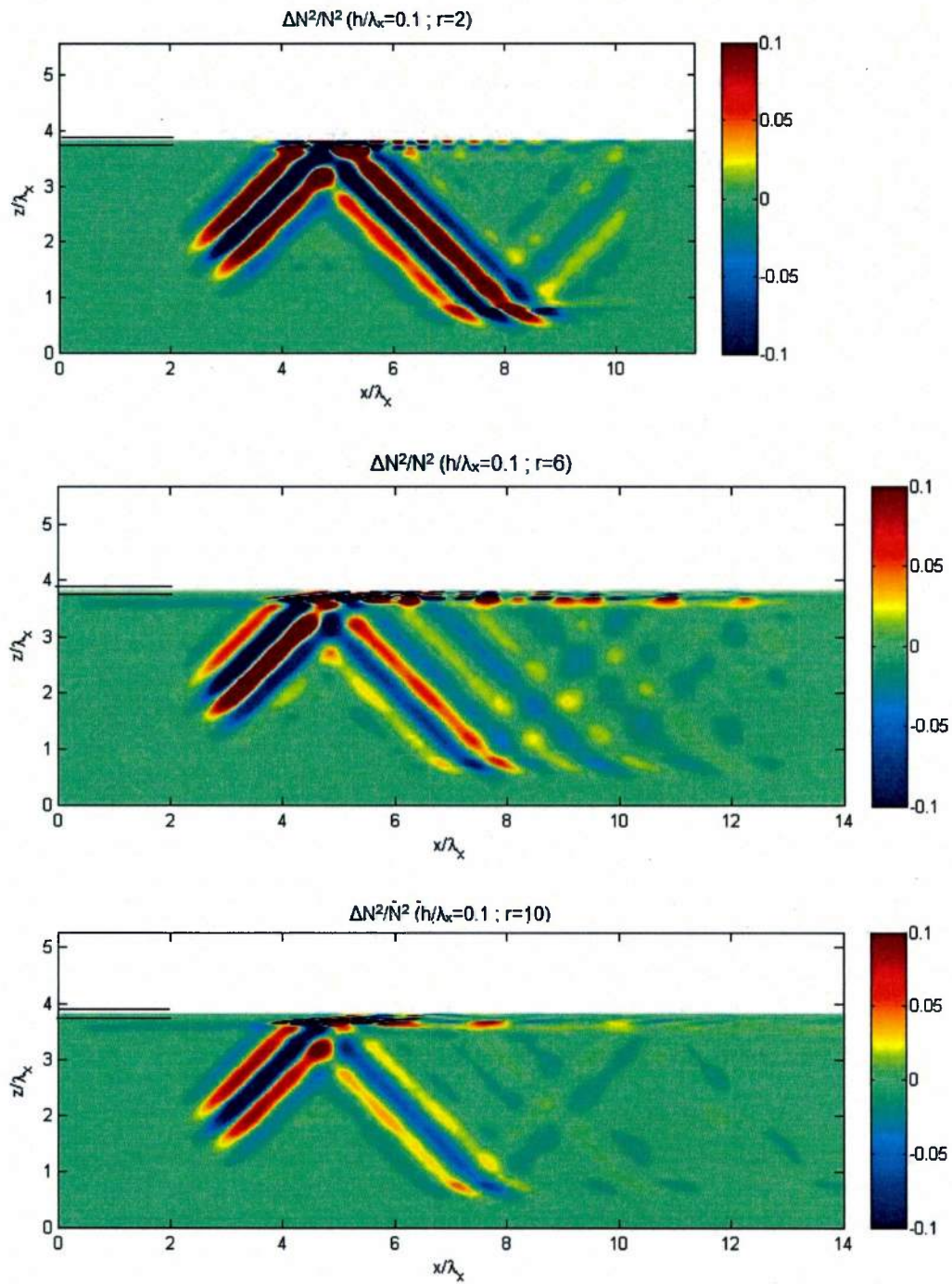


Figure 5: Snapshots of instantaneous $\Delta N^2/N^2(z)$ at steady state for $h/\lambda_x = 0.1$. Here ΔN^2 is defined as the perturbation to the buoyancy frequency associated with the wave-induced density perturbation. Top, middle and bottom panel: $r = 2$, $r = 6$, and $r = 10$, respectively. The thin horizontal solid lines delineate the interval to $z_0 \leq z \leq z_0 + h/2$, where z_0 is the pycnocline center. The upper part of each panel is blank because of the near-zero value of background stratification frequency $N^2(z)$ at these depths

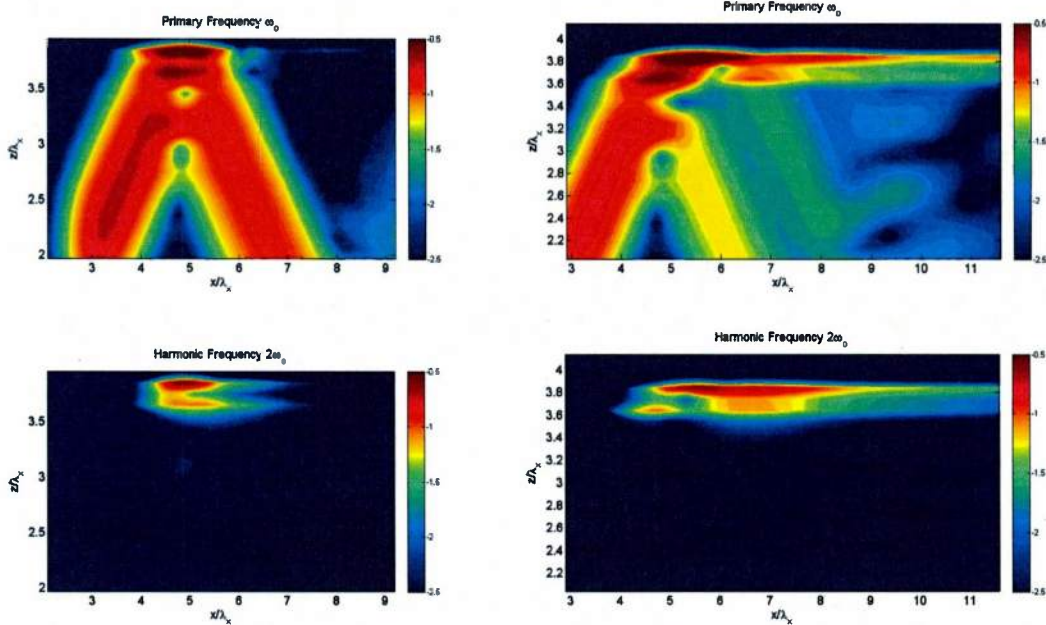


Figure 6: The normalized amplitude of the primary frequency (left) and harmonic mode (right) for simulations with $h/\lambda_x = 0.1$ and $r = 2$ (top) and $r = 6$ (bottom). The $r = 6$ case is near the interfacial wave resonance. The color scale is logarithmic. Data are sampled at a coarser spatial resolution than that of the actual simulations.

Our findings are best described in the context of the two limits of pycnocline thickness we considered, $h/\lambda_x = 0.1$ and 1, thin and thick pycnoclines respectively. A visualization of the flow structure for $h/\lambda_x = 0.1$ is shown in Figure 5. Increasing r shows a reduced capacity for the incident IWB to reflect back into the lower layer. Distinct modal structures are observed within the pycnocline for all cases, with the $r=6$ case being the most efficient in enabling the propagation of these structures, linked to harmonic frequencies, downstream within the pycnocline. At $r=2$, the pycnocline buoyancy frequency can only support evanescent harmonic modes and at $r=10$, viscous decay of the strongly refracting beam prevents strong generation of harmonics and the subsequent propagation within the pycnocline.

The thin pycnocline case of $r=6$ was found to be optimal in terms of harmonic generation and propagation as further supported by a weakly nonlinear analysis for plane internal waves, developed by Dr. Wunsch. The analysis accounts only for refraction (and not reflection) of the incident IWB. Optimal harmonic generation and propagation occur when the wavenumber and frequency of the harmonic wave are in resonance with the dispersion relation of the interfacial mode associated with the thin pycnocline. Evidence in this direction is provided by Figure 6, where the $r=6$ shows a much larger harmonic energy propagating far downstream within the pycnocline. Additional evidence of this particular resonance is provided by the agreement between theory and direct numerical simulation in terms of harmonic amplitude at different downstream locations within the pycnocline (Figure 7).

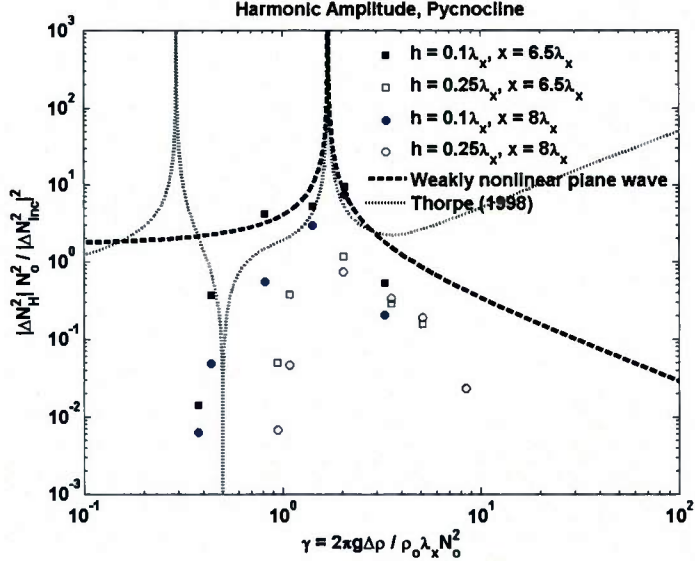


Figure 7: The dimensionless harmonic amplitude as a function of the parameter γ (a measure of pycnocline strength; $\gamma=2$ corresponds to $r=6$) for the numerical simulations with different pycnocline characteristics, along with the analytic result for a thin pycnocline. The analytical result from our weakly nonlinear theory shown as a dashed black line (also shown are results from a previous theoretical study by Thorpe based on a completely different mathematical formulation). Filled black squares show the numerical result for a pycnocline thickness $h/\lambda_x = 0.1$ at $x/\lambda_x = 6.5$, while filled blue circles show the numerical result further downstream, at $x/\lambda_x = 8$.

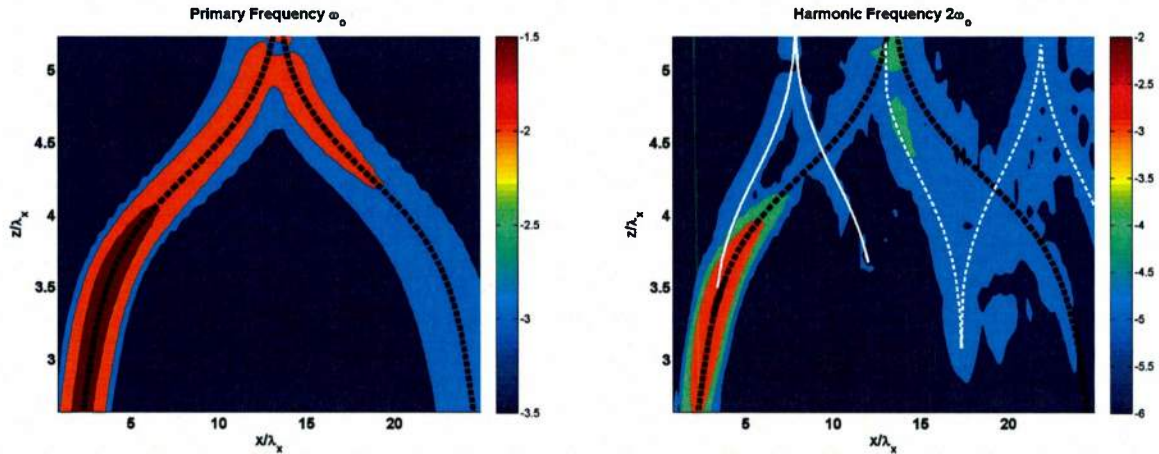


Figure 8: The amplitude of $\Delta N^2 / N^2$ for the primary (left) and harmonic (right) modes for simulations with $h/\lambda_x = 1$ and $r = 6$. The color scale is logarithmic. The dotted black line is the ray-trace path of the incident wave; the solid and dotted white lines show ray-trace paths for the harmonic frequency 2ω . Visualization window is focused on the vicinity of the pycnocline.

In the case of thick pycnoclines, harmonic generation is also dictated by refraction but not by the above resonance argument. As shown in Figure 8, the strongly refracting IWB undergoes significant viscous decay upon its entry into the pycnocline. However, non-negligible harmonic generation is observed during the initial refraction. Harmonic waves spawn off along their own propagation paths and a

complex harmonic structure is established through nonlinear wave interactions further downstream into the pycnocline. Inviscid simulations are needed to further clarify the observed flow structure and dynamics.

More detail on our findings in this topic of research may be found in the paper by Diamessis et al. (*Dyn. Atm. Ocean.* 2014).

(iii) Wake-radiated internal waves

Previous ONR-funded work by our group, enabled by our in-house designed spectral multidomain penalty method code, revealed that at sufficiently high body-based Reynolds numbers, the simulated stratified wake of a towed sphere followed a life-cycle differently than what is commonly perceived (Diamessis et al. *J. Fluid Mech.*, 2011, **671**: pg. 52-95): Buoyancy does not suppress turbulence within one buoyancy period. Instead, the horizontal shear layers are generated are sufficiently fine and strong such that secondary Kelvin-Helmholtz instabilities arise, followed by energetic secondary turbulence, which can last up to $Nt \approx O(100)$.

We investigated the impact of this prolonged secondary turbulence on internal wave radiation by the turbulent wake. Two sphere-based Reynolds number values, $Re = 5 \times 10^3$ and 10^5 were considered along with a range of internal Froude numbers, $Fr = 4, 16$ and 64 (Computational limitations at the time prevented us from reaching $Fr = 64$ at $Re = 10^5$). Our primary findings were:

- a) At high Re , the persistence time of internal wave radiation is also prolonged, with significant high-frequency waves being emitted from the wake for as times as late as $Nt = 80$ (Figure 9)
- b) There is a distinct variation in the phase-line-tilt of wake-radiated waves with increasing Re (Figure 10). At low Re , typical of the laboratory, all Fr emit waves at approximately 30° from the vertical, an angle which, according to theory, suggests that wave-radiation is a viscously driven process. It is at this angle that viscous losses are minimized. Low Re wakes are highly inefficient in depleting the mean wake flow of its energy through wave radiation. In contrast, at high Re , waves are radiated at angles in the range $[45^\circ, 55^\circ]$. Such angles optimize the extraction of momentum from the wave-generating source.
- c) Consistent with the above observation, we found that high Re wakes can extract up to a total of 6 to 8% of the initial mean wake momentum (Figure 11), unlike their low Re counterparts. Given that naval or geophysical wakes operate at Re 4 to 5 orders of magnitude higher than the largest Re considered in our study, it is likely that wave emission can be a significant source of energy that may be comparable to viscous dissipation and diapycnal mixing.

Additional results, not shown here have addressed the power law decay rates of the horizontal wavelength of the most energetic wave packets. Furthermore, we have identified a tendency for an increase in wave steepness with increasing Re and Fr (see also section (vii) and the publication by Abdilghanie and Diamessis, *J. Fluid Mech.* 2013).

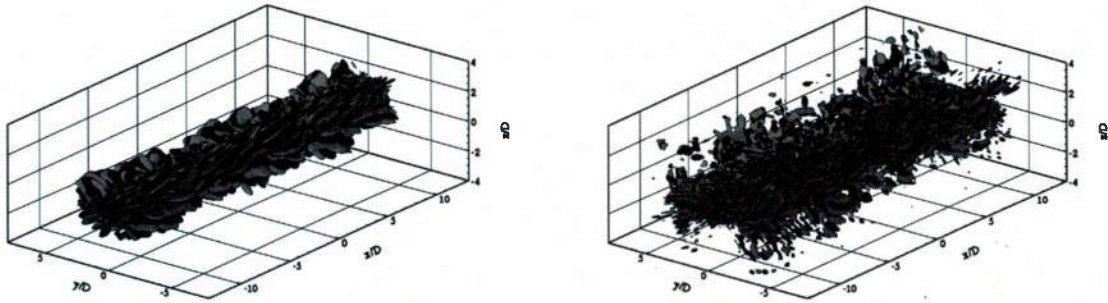


Figure 9: Isosurfaces of horizontal divergence (a measure of the internal waves radiated by the localized turbulence) for a stratified turbulent wake of a towed-sphere at sphere-based Reynolds number, $Re=10^5$, and Froude number, $Fr=4$. Shown are two different times, $Nt=20$ (left) and 80 (right). Note that a wake at the same value of Fr but at a $Re=5\times 10^3$ typical of the laboratory has no internal waves associated with it at the later time. The persistent internal wave radiation at high Re is directly connected to the secondary turbulence inside the wake core.

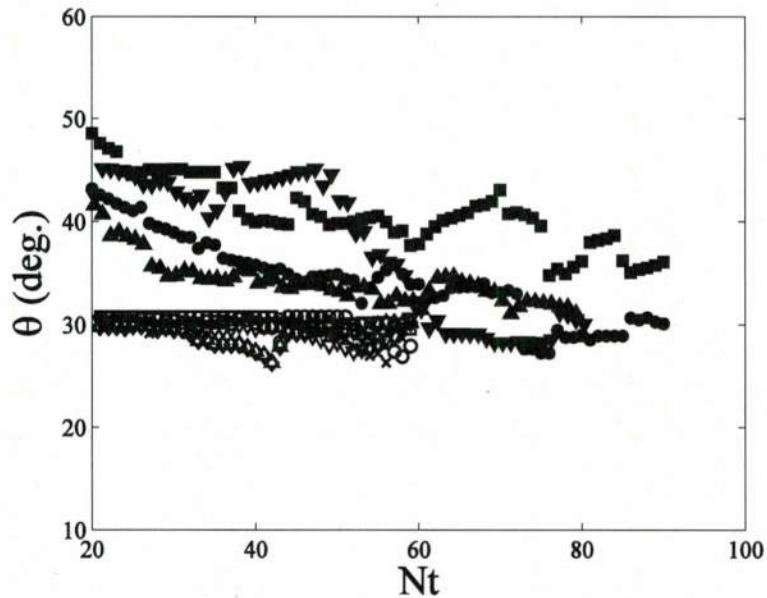


Figure 10: Phase-line tilt angle, θ , with respect to the vertical of wake-radiated internal waves for simulated stratified turbulent wakes of towed spheres at two different body-based Reynolds number values, $Re=5\times 10^3$ and 10^5 (empty and full symbols, respectively). Data are shown for three internal Froude number values, $Fr=4$, 16 and 64 . The low Re data concentrate around $\theta=30^\circ$, whereas the high Re data initially have values in the range $[45^\circ, 55^\circ]$.

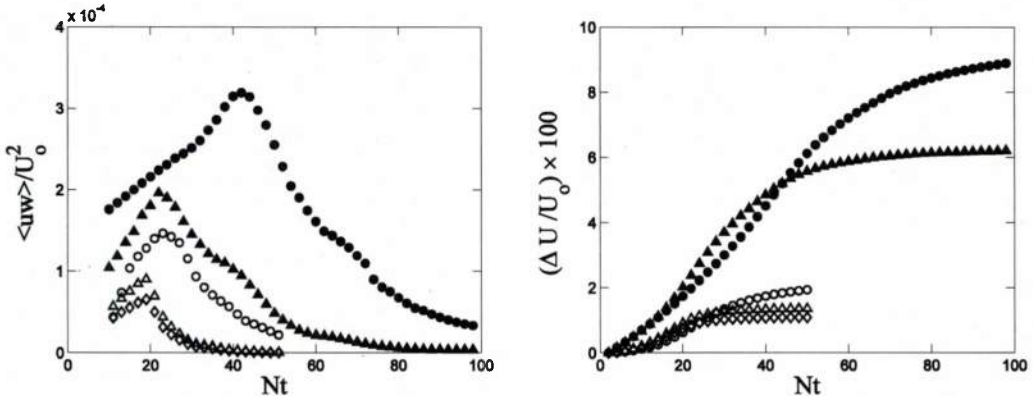


Figure 11: Left: instantaneous vertical flux of internal wave-transported horizontal momentum computed at vertically offset xy -planes, sufficiently far from the wake edge, for the cases shown in the previous figure. Empty and full symbols correspond to low and high Re , respectively (circles and triangles are $Fr=4$ and 16 cases). U_0 is the mean wake centerline velocity at $Nt=2$. Right: Time-integrated momentum transported by the stratified turbulent wake for all of the above cases.

(iv) Proper orthogonal decomposition of wake-radiated internal waves

A subset of our analysis of the wake-radiated internal wave field explored the potential of Proper Orthogonal Decomposition (POD) to probe into the generation mechanism of internal waves by a stratified turbulent wake of a towed sphere. As part of a preliminary effort, in collaboration with Profs. Roi Gurka of Ben Gurion U., Israel (now at Coastal Carolina U. in the U.S.) and Alex Liberzon at Tel Aviv U., Israel, we isolated our $Re=5\times 10^3$ and $Fr=4$ datasets and applied POD to the vorticity and horizontal divergence components on a series of snapshots on select 2-D slices on xz and yz planes within the interval $10 \leq Nt \leq 35$. Our findings are published in an article in *Physics of Fluids* (Diamessis et al. 2010) and are summarized here:

- a) Reconstruction of the streamwise vorticity, ω_x , fields on select yz planes from individual modal subranges indicated a preference of each subrange for a particular angle of wave radiation from the horizontal (figures 12 and 13). In particular, lower POD modes captured layered-like features inside the wake core and more horizontally-inclined internal wave beams, linked presumably to lower frequencies of radiation. Higher POD modes showed more fine-scale structure inside the wake core, presumably originating from turbulence, whereas the internal waves came out at angles that were more vertical.
- b) Timeseries along radial lines, inclined at increasing distance from the wake centerline, provided preliminary quantitative support for the above qualitatively observed correlation (Figure 14).

More recent work with our Israeli colleagues, funded by the US-Israel Bi-National Science foundation has provided further probing into the capacities of POD to separate turbulence and internal waves in turbulence.

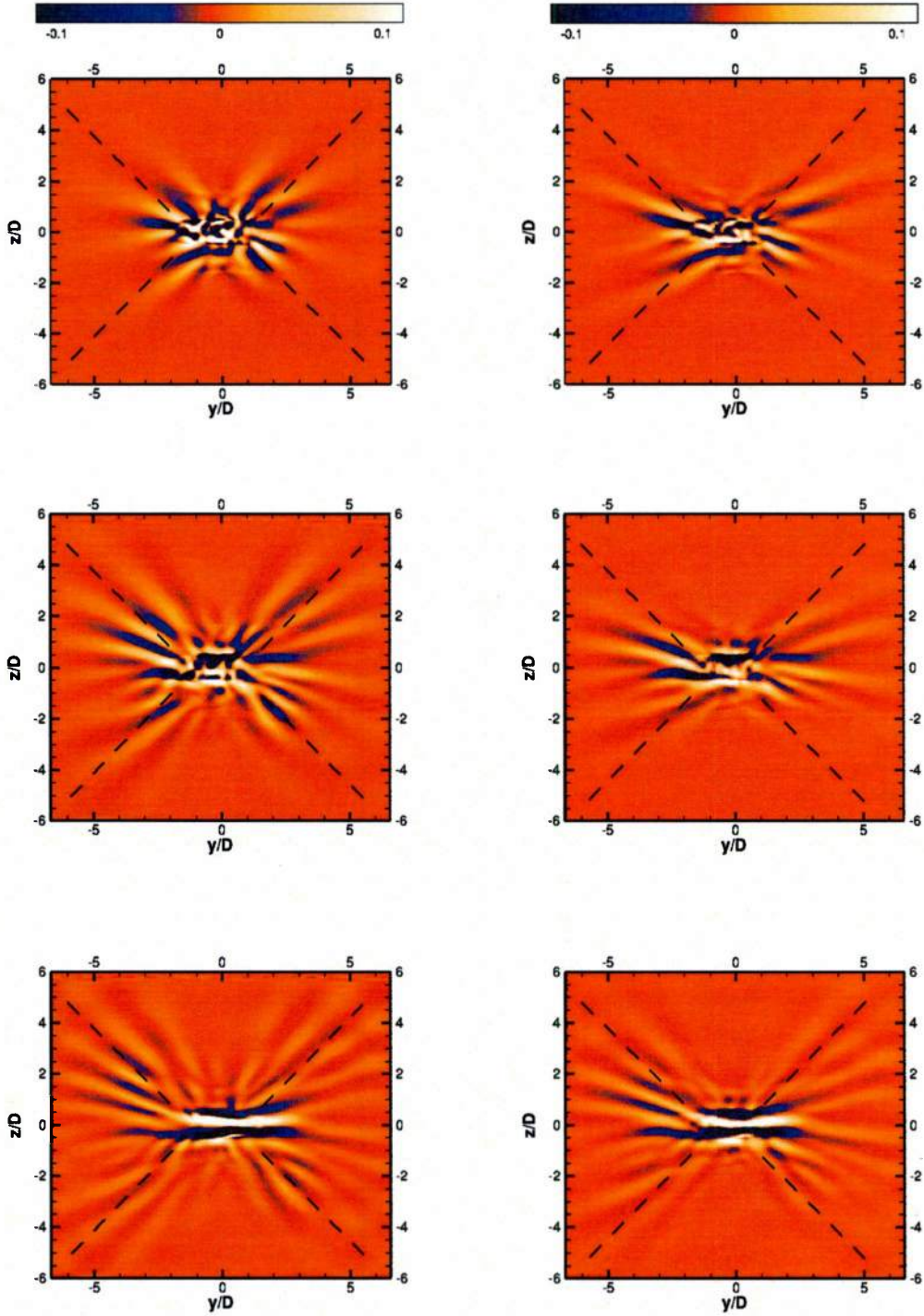


Figure 12: Full (panels (a), (c) and (e)) and reconstructed (panels (b), (d) and (f)) ω_x field on a yz plane located at the middle of the wake-centerline. Reconstruction is performed for POD modal subrange 1–3. Top panel: $Nt=15$. Middle panel: $Nt=25$. Bottom panel: $Nt=35$. The dashed black lines are inclined at 45° to the horizontal.

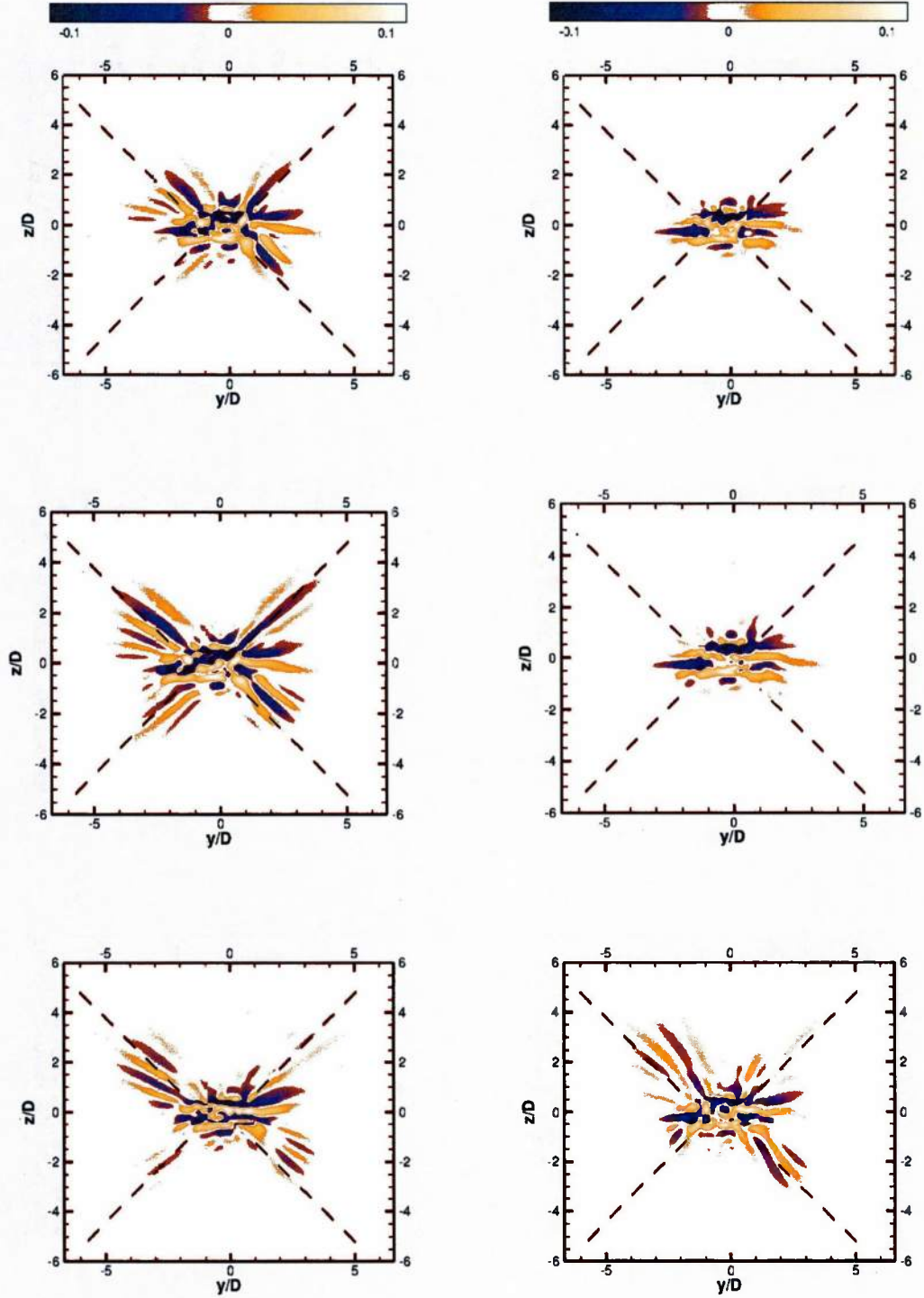
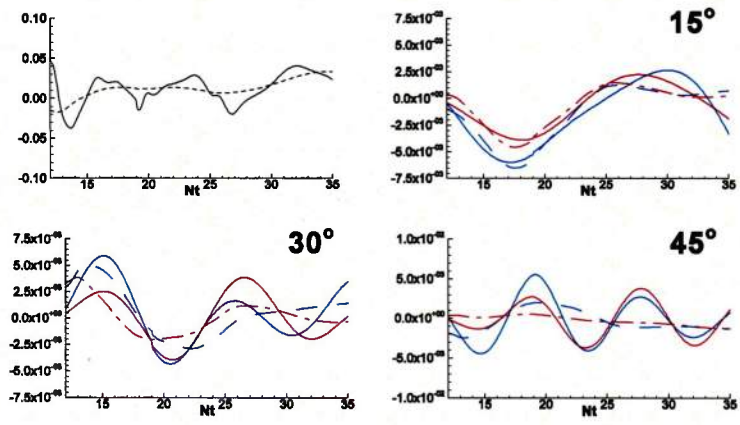
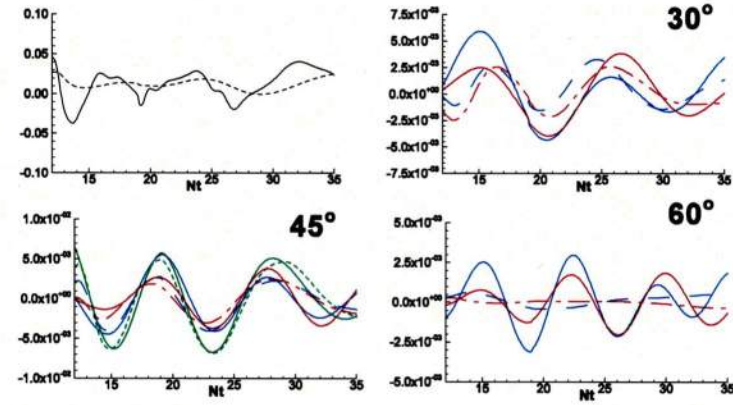


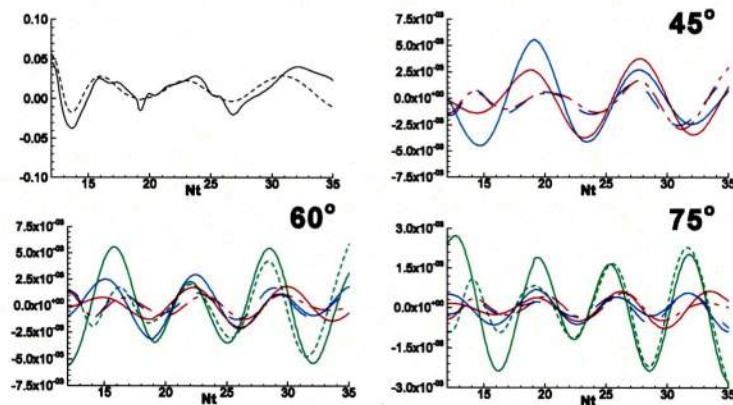
Figure 13: Reconstructed ω_x field on the same yz plane as in the previous figure located at the middle of the wake-centerline. Reconstruction is performed for POD modal subrange 4–6 (left column) and 7–10 (right column). Top panel: $Nt=15$. Middle panel: $Nt=25$. Bottom panel: $Nt=35$. The dashed black lines are inclined at 45° to the horizontal.



(a)



(b)



(c)

Figure 14 (previous page): Timeseries of the full and reconstructed ω_x field on the same yz plane as the previous figure obtained from virtual sensors positioned at different azimuthal angles on the 1st quadrant. Sub-figures (a), (b) and (c) correspond to modal subranges 1-3, 4-6 and 7-10, respectively. In each sub-figure the top-left panel shows time series at wake centerline. The remaining three panels of each subfigure show signals at specified azimuthal angles. Blue and red lines correspond to data at $r=3D$ and $4D$, respectively. Black lines are used only for the data at the wake centerline in the top panel. Solid lines represent full flow field and nonsolid lines represent the reconstructed flow field.

(v) Eulerian mean flows in a subsurface reflecting internal wave beam

As a first step in the second leg of our ONR-funded research and as part of an ongoing effort to understand the fate of turbulence-radiated internal waves far from their source, this study examined nonlinear effects in the reflection of a 2-D finite-amplitude internal wave beam (IWB) off a free-slip surface, a model for the ocean surface on a calm day (Figure 15). A linear stratification was considered, along more complex ones. We focused on mean flow formation but also investigated the formation of frequency-harmonics of the primary beam and the potential for parametric subharmonic instability. In all these efforts, a uniform linear stratification was considered. A subset of our analysis considered similar effects in a configuration where a mixed layer laid above the linear stratification. The base of the mixed layer operated in an equivalent manner as the free-slip surface.

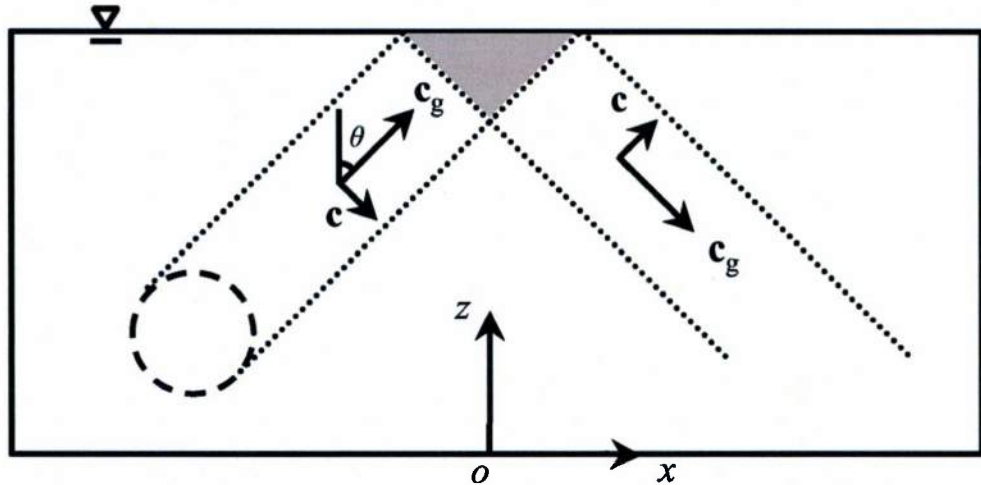


Figure 15: Schematic of a 2-D IWB reflecting off a free-slip surface.

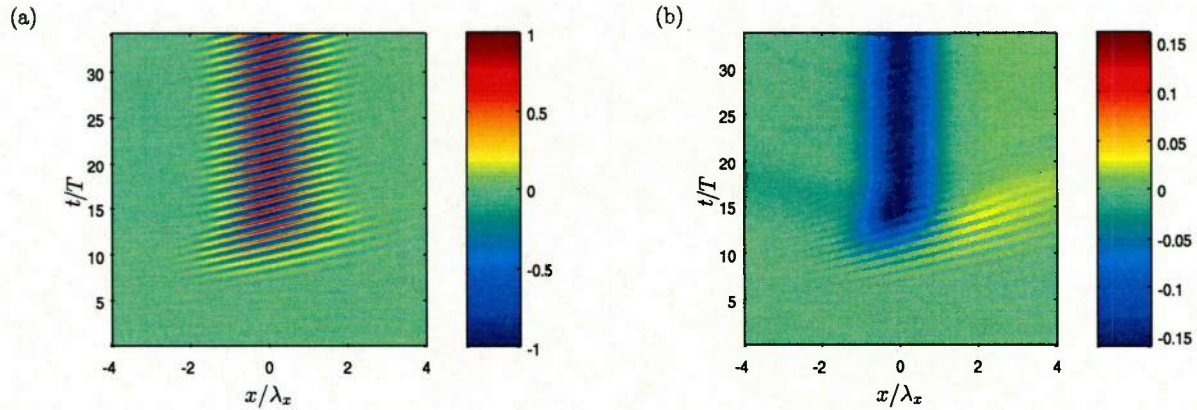


Figure 16: (a) Streamwise position vs. time diagram of u-velocity at the surface off which the IWB reflects. (b) Time-averaged IWB-induced mean flow.

The primary findings of this study were the following:

- We have identified the structure of the IWB-induced Eulerian mean flow over the corresponding region of the water column. A persistent current, between 10 and 50%, of the horizontal phase speed of the beam is established at the surface (figures 16 (a) and (b)).
- The amplitude of the mean Eulerian surface current is found to scale linearly with the IWB amplitude A and $\tan\theta$, where θ is the phase-line tilt of the beam w/r to the vertical (Figure 17). Strongly hydrostatic beams (θ very close to 90°) produce the strongest mean flows. Very good agreement with the theoretical predictions of Tabaei et al. (*J. Fluid Mech.* 2005, **526**: pg 217–243) is found for all simulated waves.
- For sufficiently high-amplitude beams, a parametric subharmonic instability is observed after a long enough time (Figure 18). Significant energy of the primary IWB is spawned off to secondary beams of lower frequency, which are more horizontally inclined. Frequencies and wavenumbers of the primary and secondary beams are found to match theoretically prescribed resonance conditions very closely.

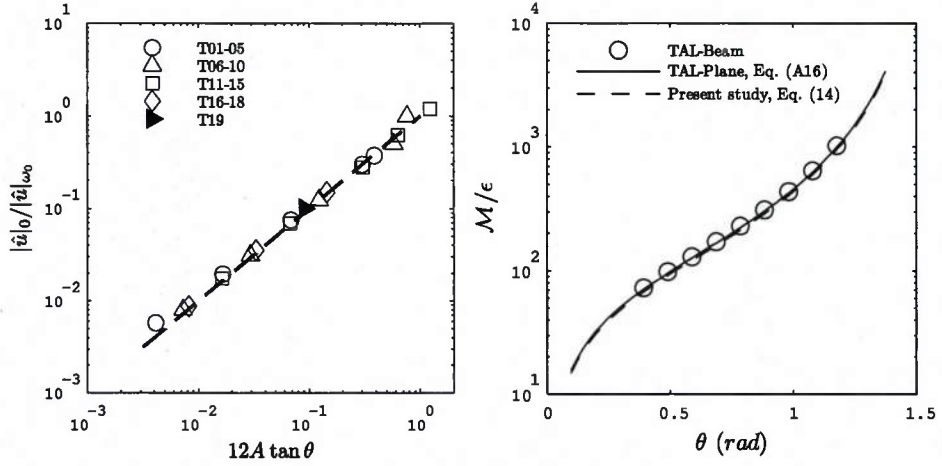


Figure 17: Left panel: Magnitude of IWB-induced mean current at the free surface, normalized by the magnitude of the maximum horizontal velocity inside the primary IWB, as a function of beam amplitude A and angle to the vertical θ . Numerical computed mean currents vs. the theoretical estimates of Tabaei et al. (2005) as a function of angle θ .

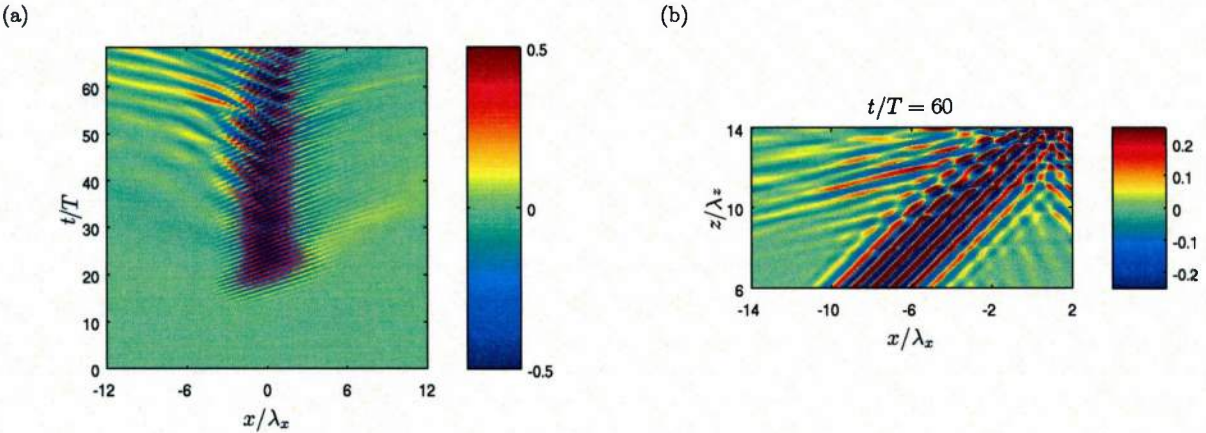


Figure 18: (a) Streamwise position vs. time diagram of instantaneous horizontal velocity at the surface for a very high amplitude beam ($A=6.8\%$). Time and position are normalized with IWB period T and horizontal wavelength λ_x , respectively. Parametric subharmonic instability (PSI) manifests itself in the form of more horizontal like isophase lines at $t/T \geq 50$. (b) xz -contour plot of horizontal velocity at late times for a PSI-prone IWB. The subharmonic waves are more horizontally inclined and are easily spotted spawning off to the left of the primary beam.

(vi) Lagrangian mean flows in a surface reflecting internal wave beam

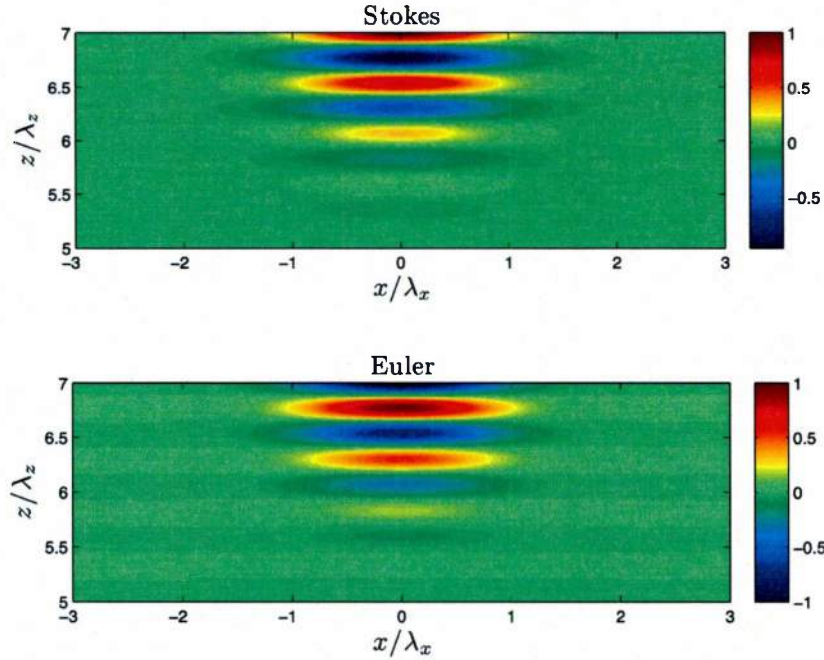


Figure 19: Leading order Lagrangian mean drift (top) vs. Eulerian mean flow for the reflecting IWB in figure 16. Both sets of contour values are normalized by U_o^2/c_x , where U_o is the maximum horizontal velocity in the incident wave and c_x is its horizontal phase speed. The two different types of mean flow cancel each other out to almost machine precision.

As we continue to probe into the subsurface signature of the wake-radiated internal wave field, we have further extended our study of the reflection of an individual IWB at a free-slip surface to explore for the Lagrangian mean flows in the reflection zone. Understanding such Lagrangian effects is imperative to quantify the true mean flow (as its Eulerian component does not suffice in this regard). Furthermore it provides insight into the internal wave-driven Lagrangian drift of surface-particulates.

Borrowing elements of surface wave theory, we have found that the Stokes drift fully cancels out its Eulerian counterpart in the reflection region (figure 19). Any resulting Lagrangian particulate drift should be of second (higher) order than each of these mean flow components. Application of a high-accuracy (Fourier-Legendre in space, 4th order Runge-Kutta in time) particle tracking technique to the flow fields used in Zhou and Diamessis (2013), confirms this claim (figure 20). However, the dispersion becomes significant when PSI ensues (figure 21).

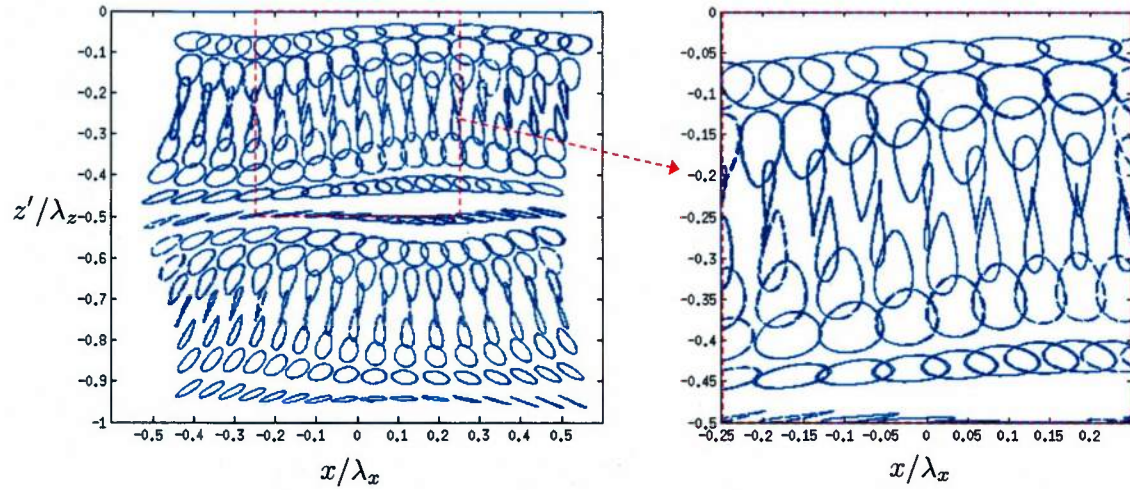


Figure 20: Tracer particle orbits for five wave periods within a reflecting IWB. No noticeable mean drifts are observed. Any higher-order Lagrangian drift is very weak for a stable reflecting IWB at this particular wave set-up.

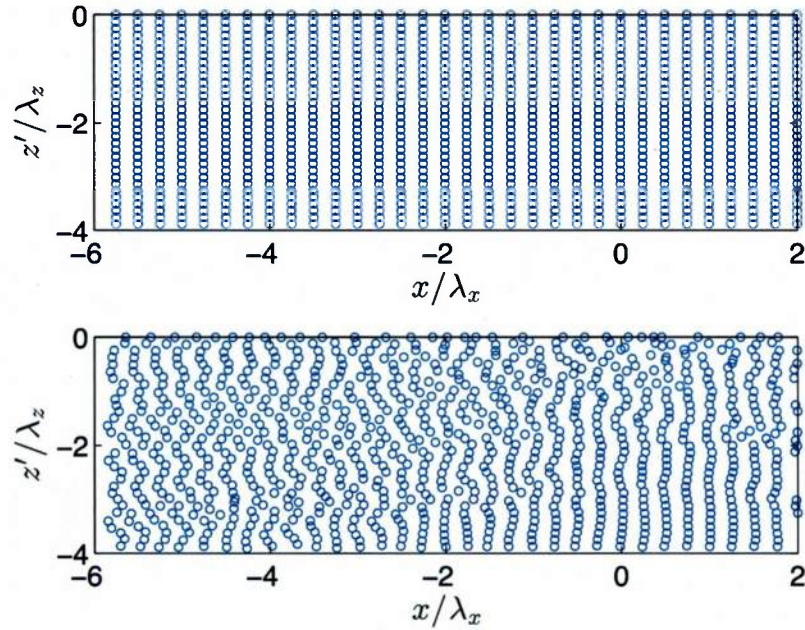


Figure 21: Tracer particle displacements at the initial time (top) and after one wave period (bottom) for the PSI-prone reflecting IWB of figure 16. Any higher-order Lagrangian drift is very weak for a stable reflecting IWB.

(vii) Subsurface signature of the wake-radiated internal wave field.

This is ongoing work which we expect to wrap up in late summer/early fall 2014 and should give rise to one more manuscript. We consider the same cases as in section (iii), though in deeper and wider domains and augmented with a $Fr=64$ simulation at the higher Reynolds number. Focusing on a uniform stratification, which extends up to the surface, we aim to identify the time (in buoyancy units) of when the strongest strains emerge at the surface above the submerged wake. Furthermore, we seek to parameterize these strains as a function of Re and Fr . In addition, we are exploring the variation in observed surface wavelengths and their orientation across all runs while we are also investigating surface signatures of interest to remote sensing experts. The latter effort is in close collaboration with Prof. Bill Philpot at CEE-Cornell.

The first step in analyzing the (sub)surface signature of the wake-radiated internal wave field has consisted of calculating the surface strain field, as represented by the horizontal divergence Δ_z . Examination of the $Re=5\times 10^3$ dataset indicates that the peak strain rate, across all Fr , scales as $Fr^{-1/2}$ whereas the corresponding arrival time $t/(D/U)$ scales as $Fr^{2/3}$ (figure 22). The equivalent analysis at $Re=10^5$ is still underway. A first finding is that the internal wave induced strains persist for a longer time and reach a peak value that is $O(10)$ larger than their low Re counterpart.

A key component of ongoing work aims to quantify the characteristic time and length scales of the near-surface flow field through 1-D and 2-D continuous wavelet transforms. On account of the significant vertical distance separating the edge of the wake and the free surface, significant dispersion (variation in frequency) is observed with lateral offset at the surface (figure 23). Finally, figure 24 shows a sample of 2-D wavelet analysis of the surface strain field with a distinct resonance occurring at a particular horizontal wavescale.

What is most intriguing is the structure of the wake-radiated internal wave field at $Re=10^5$ and $Fr=64$ (figure 25). Along with the above dispersion, the wake energy released into the internal wave field is sufficiently large that the emitted waves are so steep that they are very close to breaking. The implications of such potential breaking for surface signatures will be explored in the near future.

The surface signature of wake-radiated internal waves may be remotely detected through various means, one of which is the characterization of slicks of surface surfactants. By solving for a pure 2-D advection equation on the surface we can observe the evolution of a passive scalar (with an initially uniform distribution) as affected by the wave-induced surface velocity field. The slick pattern mimics that of the reflecting internal waves. Most importantly though, the enrichment ratio (instantaneous over initial concentration) of the passive scalar field is found to exceed the critical value of 1.05 at $Re=10^5$ (figure 26) which implies enhanced remote detectability of the surface signature of the waves due to strong visible contrast

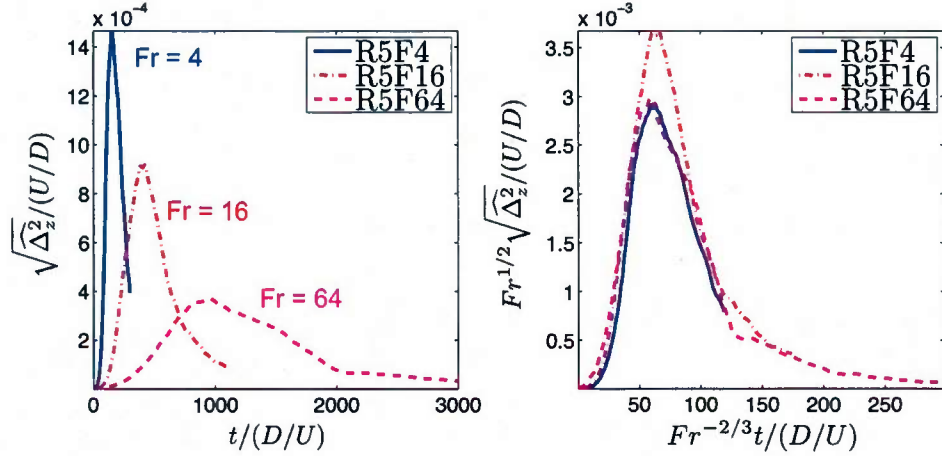


Figure 22: Surface-averaged internal wave-induced strain at the free surface for the $Re=5\times 10^3$ datasets at three different Fr values (left). Right panel indicates a preference for a preferred Fr -scaling for strain magnitude and time of observation of maximum strain at the surface.

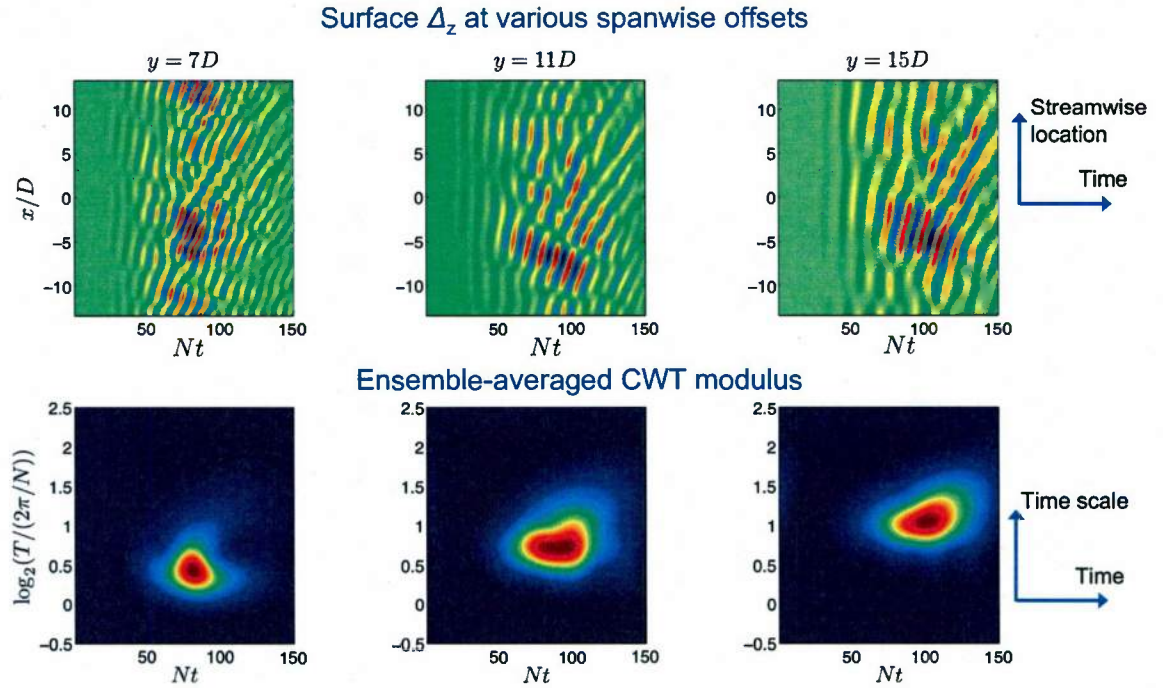


Figure 23: Top: Streamwise position vs. time (in buoyancy units) diagrams of horizontal divergence at the free surface for the $Re=5\times 10^3$ and $Fr=4$ simulation at three different lateral offsets. Bottom: Corresponding x -averaged period. Notice the steady change in wave period with lateral offset, an indicator of frequency dispersion in the original wake-radiated internal wave field.

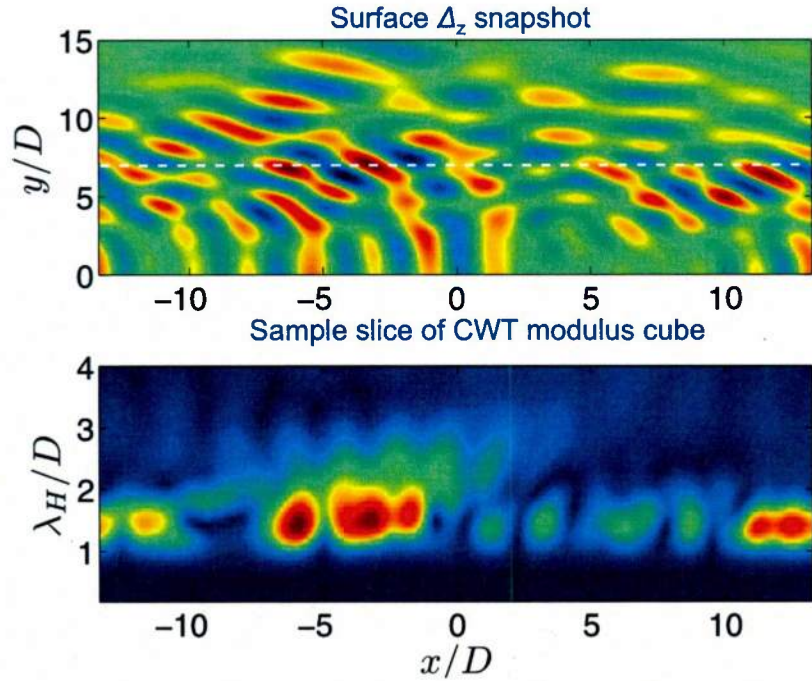


Figure 24: Top: Snapshot of surface horizontal divergence for the same simulation as in the previous figure. Only the positive y -half of the free surface is shown. Bottom: 2-D transect from the continuous wavelet transform modulus cube at the y/D offset corresponding to a white line in the top panel. Red regions of strong resonance correspond to individual wave packets of horizontal wavelength λ_H/D .

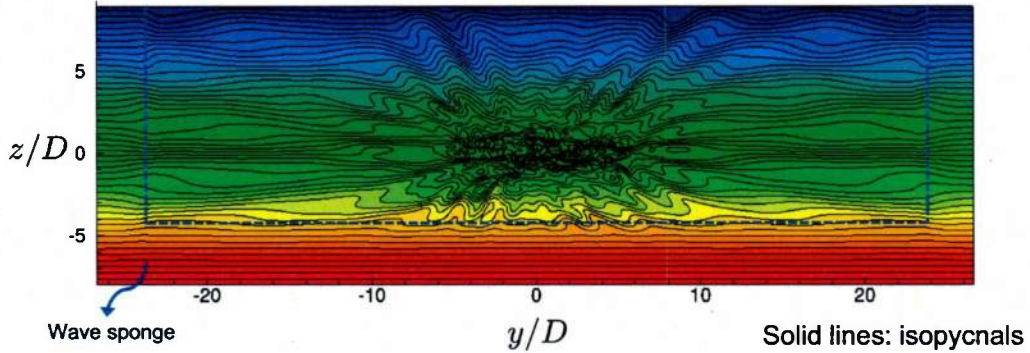


Figure 25: Isopycnal contours from an yz slice from the $Re=10^5$ and $Fr=64$ simulation at $Nt=45$. Notice the very steep, nearly overturned, isopycnals in the radiated internal wave field at non-negligible distances from the wake core. Whether these waves break is a topic of current investigation.

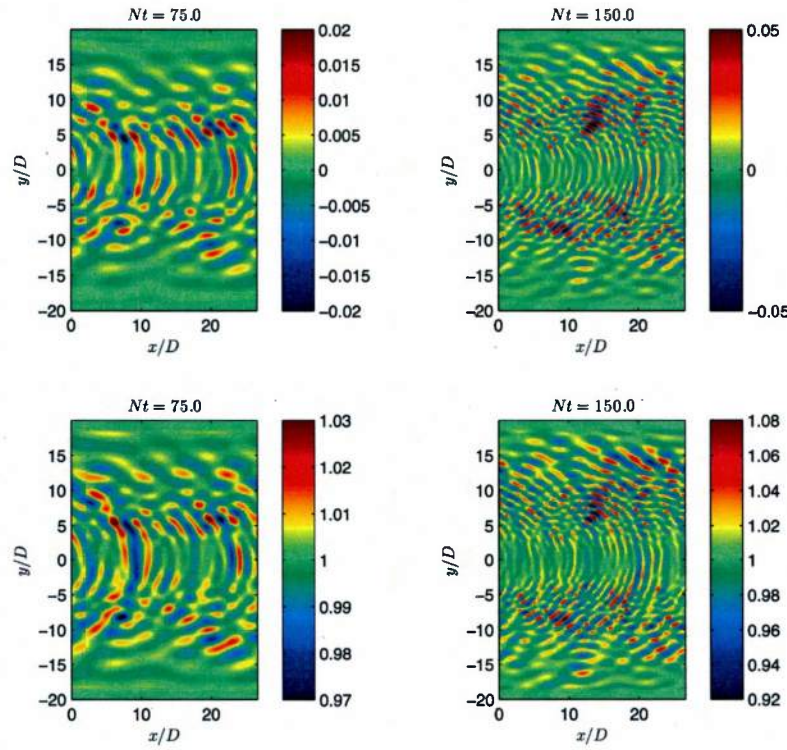


Figure 26: Top panel: Horizontal divergence field at two different times for the $Re=10^5$ and $Fr=4$ simulation. Bottom panel: Corresponding concentration fields resulting from a 2-D advection simulation with an initial condition of uniform scalar concentration (values normalized with initial concentration, a quantity defined as enrichment ratio in remote sensing). Notice how the enrichment ratio exceeds the critical value of 1.05 at late times, which suggests enhanced likelihood of remote detectability.

Ongoing/Future Work

Current work is focused on analyzing the full subsurface signature of wake-radiated waves for the six pairs of points in the (Re, Fr) parameter space identified in section (vii) of this proposal. Completion of this effort is anticipated by late summer 2014, to be followed by the write-up of a relevant publication. Through the assistance of DoD-PETT we are working on profiling and optimizing the performance of our parallel spectral multidomain penalty method solver for the incompressible Navier-Stokes equations. Enabled by a DoD Frontier project, spearheaded by Prof. Steve de Bruyn Kops at U. Mass. Amherst, we are engaged in regular discussions on stratified turbulence and have begun implementing direct numerical simulations (with Prof. de Bruyn Kops) initialized with our own implicit L.E.S. data. In parallel, through Frontier computational resources, we have initiated three massively parallel stratified wake simulations at $Re=4\times 10^5$ and $Fr=4, 16$ and 64 . Run completion is expected in late October 2014 with the associated analysis completed by late winter 2015. The analysis will aim to quantify the Re -scaling of properties of the mean wake and the radiated internal wave field.

Personnel

This ONR grant has supported two Ph.D. students. Dr. Ammar Abdilghanie received his Ph.D. in Fall 2010. Following postdoctoral appointments at the U. of Washington and at Argonne National Laboratory, he is now a member of Halliburton's R&D department. Mr. Qi Zhou is the PhD student currently funded by the extension of this grant. He is expected to graduate in late spring/early summer 2015.

Two undergraduate students have also been involved in this effort, funded by the PI's NSF CAREER award grant and internal support from the Cornell College of Engineering: Mr. Ian Delwiche and Mr. M. Paul Richter. Mr. Delwiche also spent two summers and one winter break working as an intern in the Johns Hopkins U. Applied Physics Laboratory, under the supervision of our collaborator Dr. Scott Wunsch.

Publications generated by this project

A.M. Abdilghanie (2010) "A numerical investigation of turbulence-driven and forced generation of internal gravity waves in stratified mid-water". *PhD thesis*, Cornell University.

A.M. Abdilghanie and P.J. Diamessis (2012) "On the generation and evolution of numerically simulated large-amplitude internal gravity wave packets". *Theor. Comp. Fluid Dyn.*, **26**: 205-2245.

A.M. Abdilghanie and P.J. Diamessis (2013) "The Internal Wave Field Emitted by a Stably Stratified Turbulent Wake", *J. Fluid Mech.* ; 720, pg. 104-139.

P.J. Diamessis, R. Gurka R. and A. Liberzon (2010) "Spatial characterization of vortical structures and internal waves in a stratified turbulent wake using proper orthogonal decomposition". *Phys. Fluids*, **22**: article 086601.

P.J. Diamessis, S. Wunsch, I. Delwiche I. and M.P. Richter (2014) “Nonlinear generation of harmonics through the interaction of an internal wave beam with a model oceanic pycnocline ” , *Dyn. Atm. Ocean.*, 66, 2014, pg. 110-137.

Q. Zhou and P.J. Diamessis (2013) “Reflection of an Internal Gravity Wave Beam off a Horizontal Free-Slip Surface” , *Phys. Fluids* ; 25, Article 033601.

Q. Zhou and P.J. Diamessis “Lagrangian flows within reflecting internal gravity waves at a free-slip surface” (2014), (In preparation for *Phys. of Fluids*).